Talanta 104 (2013) 140–148

Contents lists available at SciVerse ScienceDirect

Talanta

journal homepage: www.elsevier.com/locate/talanta

Comparison of on-line detectors for field flow fractionation analysis of nanomaterials

A.J. Bednar [a,*], A.R. Poda [a], D.M. Mitrano [b], A.J. Kennedy [a], E.P. Gray [c], J.F. Ranville [b], C.A. Hayes [d], F.H. Crocker [a], J.A. Steevens [a]

[a] US Army Engineer Research and Development Center, Environmental Laboratory, 3909 Halls Ferry Rd., Vicksburg, MS 39180, USA
[b] Department of Chemistry and Geochemistry, Colorado School of Mines, Golden, CO 80401, USA
[c] Department of Civil and Environmental Engineering, Colorado School of Mines, Golden, CO 80401, USA
[d] Badger Technical Services, Vicksburg, MS 39180, USA

ARTICLE INFO

Article history:
Received 4 June 2012
Received in revised form
2 November 2012
Accepted 7 November 2012
Available online 19 November 2012

Keywords:
Nanomaterials
Detection
Sizing
Field flow fractionation
ICP–MS
ICP–AES

ABSTRACT

Characterization of nanomaterials must include analysis of both size and chemical composition. Many analytical techniques, such as dynamic light scattering (DLS), are capable of measuring the size of suspended nanometer-sized particles, yet provide no information on the composition of the particle. While field flow fractionation (FFF) is a powerful nanoparticle sizing technique, common detectors used in conjunction with the size separation, including UV, light-scattering, and fluorescence spectroscopy, do not provide the needed particle compositional information. Further, these detectors do not respond directly to the mass concentration of nanoparticles. The present work describes the advantages achieved when interfacing sensitive and elemental specific detectors, such as inductively coupled plasma atomic emission spectroscopy and mass spectrometry, to FFF separation analysis to provide high resolution nanoparticle sizing and compositional analysis at the μg/L concentration level, a detection at least 10–100-fold lower than DLS or FFF–UV techniques. The full benefits are only achieved by utilization of all detector capabilities, such as dynamic reaction cell (DRC) ICP–MS. Such low-level detection and characterization capability is critical to nanomaterial investigations at biologically and environmentally relevant concentrations. The techniques have been modified and applied to characterization of all four elemental constituents of cadmium selenide–zinc sulfide core–shell quantum dots, and silver nanoparticles with gold seed cores. Additionally, sulfide coatings on silver nanoparticles can be detected as a potential means to determine environmental aging of nanoparticles.

Published by Elsevier B.V.

1. Introduction

Nanotechnology offers potential advancements for both industrial and commercial sectors, including useful products either when used alone or when integrated with other materials into larger products (e.g., consumer goods, foods, pesticides, pharmaceuticals, and personal care products, among others). Specifically, it is particularly important to develop improved detection techniques for metal-containing nanoparticles (NPs) since they are the fastest growing category of engineered NPs (ENPs). With the list of applications growing rapidly, the use of nanomaterials could potentially impact environmental systems. In fact, a number of life cycle assessments concluded that a significant amount of metal bearing NPs is likely to enter aquatic systems [1–3]. Despite the rapid progress, use, and probable release of nanoproducts to the environment, questions remain on the potential toxicological risk to the biome [4,5].

Understanding nanoparticle fate in the environment is difficult, due in part to challenges associated with detecting small amounts in complex environmental and biological matrices. These complex, heterogeneous matrices may confound detection of very low (μg/L or less) levels of engineered nanomaterials. Spectrometry techniques, including a very new method, single particle ICP–MS (SP–ICP–MS), have been applied for the detection of NP determining both concentration and size simultaneously [6–8]. However, the most commonly used detection and characterization methods available to assess particle concentration and size distributions are not adequate for the study of NPs in complex systems or at low concentrations [9]. These include microscopy [10], chromatography [11], centrifugation [12], laser light scattering [13], and filtration [14,15]. One particular analytical challenge is distinguishing engineered nanoparticles from other constituents of the matrix such as natural particles, humic substances, and debris [16]. Perhaps the major problem identified

* Corresponding author. Tel.: +1 601 634 3652.
E-mail address: anthony.J.Bednar@usace.army.mil (A.J. Bednar).

0039-9140/$ - see front matter Published by Elsevier B.V.
http://dx.doi.org/10.1016/j.talanta.2012.11.008

with most techniques relates to method sensitivity, which is generally insufficient compared to environmentally and toxicologically relevant concentrations (μg/L to ng/L ranges) [17,18].

One of the most commonly used approaches to study nanoparticles is microscopy, either Transmission Electron Microscopy (TEM) or scanning probe microscopy. Theoretically, microscopy offers the ultimate sensitivity, with the ability to detect/image a single nanoparticle; however, accomplishing this practically is equivalent to the proverbial 'needle in a haystack'. These techniques create images of single particles but their shortcomings include unrepresentative sampling, changes during the preparative process (i.e., agglomeration), and inability to find particles in very dilute samples. Another common approach that has long been used to study colloidal solutions is Dynamic Light Scattering (DLS), which measures the particle hydrodynamic diameter. However, limitations for the study of nanoparticles are numerous including: poor sensitivity at dilute concentrations, nonselective material detection, failure to differentiate between nanoparticles and other matrix components, and the inability to reliably quantify the relative proportions of particle or aggregate sizes in multi-modal distributions. Multi-modal populations are particularly problematic for DLS as intensity-normalized results will characteristically be disproportionately skewed to the larger particles/aggregates in suspension even if smaller sizes predominate. Furthermore, many analytical techniques have difficulty distinguishing organic coatings that may be present on nanoparticles.

Field flow fractionation (FFF) consists of a suite of high resolution sizing techniques which allows separation and sizing of macromolecules, submicron colloids, and nanoparticles of 1–100 nm, depending on the type of field applied and mode of operation [19]. The separation process is similar to chromatography except that it is based on physical forces (e.g., diffusion) as opposed to chemical interactions. Particle separation is preformed in a thin channel with laminar flow under the influence of a perpendicular field. Depending on the type of analysis that is being performed, a different member of the FFF family would be chosen to achieve optimal separation results. The three techniques that are the most commercially available and thus most commonly used include thermal, sedimentation and flow FFF. Applications of FFF have become increasingly diverse in the recent years to include separation and characterization of proteins [20], polymers [21], cells [22], natural nanoparticles [23] and more recently manufactured nanoparticles [24].

Flow FFF (FlFFF) was chosen for this research because it is the most widely used subset of techniques for environmental analysis and is highly versatile for a range of both natural and manufactured NPs. As outlined in Baalousha and Lead [25], the increased use of FlFFF can be related to the wide size range that can be fractionated either of natural colloids (1–1000 nm) or natural and manufactured NP (1–100 nm) [26]. Many FFF techniques, including FlFFF, are also adaptive, allowing the ability to change carrier solutions with respect to pH and ionic strength as to match the carrier solution with sample composition [27], and the possibility of both on-line hyphenation to a wide range of detectors as well as collection of sample fractions for further off-line analysis [25,28–31,8].

UV absorbance is a common non-destructive detector for on-line processes; therefore, FFF–UV hyphenation has been used extensively. However, with the sensitivity limited generally to particle concentrations in the mg/L range, FFF–UV is not suitable for many environmental studies since aggregation behavior may be vastly different at low μg/L levels where the probability of particle-to-particle collisions is lower. Additionally, the UV detector lacks specificity, even when multiple wavelengths are employed. Interfacing FFF with ICP–MS or ICP–AES, however, allows element specific detection at trace concentration levels [32] when studying metal-containing NP [33]. Several reviews have been published discussing the broad range of environmental [32,34], biological [35,36], and nanoparticle [18,37–39] applications for FFF–ICP–MS [40]. Furthermore, the capability of multi-metal analysis is an added benefit when using these detection techniques.

Though literature is scarce to engineered nano-specific studies, there is a growing potential for the use of FFF in nanoecotoxicity studies with increasing interest concerning characterization methodology for environmental and biological risk evaluation. Notably, recent studies to characterize quantum dots [41] and NP [42–44] in biological media before and after exposure, as well as environmental samples [28,45,46] have shown promising results when using FFF–ICP–MS and FFF–ICP–AES. The resultant hyphenated techniques of FFF–ICP–MS and FFF–ICP–AES described in the present study provide nanoparticle detection, sizing, and compositional analysis capabilities at the μg/L level for multiple elements present within the nanoparticle, which is critical to environmental and toxicological investigations of nanomaterials [14,40]. We demonstrate the advantages of using dynamic reaction cell ICP–MS and ICP–AES detectors for non-metallic analytes present in nanomaterials in addition to standard ICP–MS in comparison to UV absorbance detection. The methodology developed in the current work expands detection capabilities for multiple components of nanoparticle systems, including core–shell gold–silver nanoparticles, Cd–Se–Zn–S quantum dots, and silver nanoparticles after sulfidation, these methods can be used for more descriptive nanoparticle fate and characterization.

2. Materials and methods

2.1. Reagents and nanoparticles

All nanoparticles were obtained from commercially available sources. Aqueous NanoXact silver nanoparticle suspensions (nominal primary particle sizes of 10, 20, 30, and 60 nm) were purchased from Nanocomposix (San Diego, CA) at 20 mg/L stock concentration stabilized with either citrate or tannic acid. These particles were nearly monodisperse in size as determined by Transmission Electron Microscopy, DLS, and FFF–ICP–MS analyses [42]. Aqueous suspensions of gold nanoparticles were purchased from the National Institute of Standards and Technology (NIST, Standard Reference Materials 8011, 8012, and 8013) at nominal 50 mg/L stock concentrations. These particles were also monodisperse as determined by Atomic Force Microscopy, DLS, and FFF–ICP–MS analyses.

All nanosilver and nanogold stock solutions were diluted in 18.2 MΩ cm deionized water and used immediately after dilution. UV–vis spectra were obtained for the Ag and Au particles using a Beckman-Coulter DU 800 spectrometer. Cadmium selenide–zinc sulfide core–shell quantum dots (eFluor^{TM}605NC carboxyl functionalized) were purchased from eBioscience, Inc. (San Diego, CA) at a reported 10 μM concentration stabilized with DSPEPEG lipid (1,2-distearoyl-sn-glycero-3-phosphoethanolamine-*N*-[carboxy-(polyethylene glycol)-2000]) and received in 0.1 M borate, 0.3 M NaCl, ~0.01% Sodium Azide at pH 8.3. This stock solution was diluted 1:200 in 18.2 MΩ-cm deionized water for all FFF analyses presented below (which results in cadmium, zinc, selenium, and sulfur concentrations of 7.73, 4.12, 1.72, and 43.9 mg/L, respectively, as determined by ICP–MS and ICP–AES analysis).

2.2. Asymmetrical FFF(AF4) and DLS

AF4–UV and AF4–light scattering analysis was performed to provide a comparison to the use of ICP–MS and ICP–AES detection

described below. For these experiments an asymmetrical field flow fractionation system (AF4) from Postnova Analytics (Salt Lake City, UT) was interfaced to a Shimadzu UV–vis detector and a Malvern NanoZS (Malvern, UK). The AF4 channel was fitted with a 10 kDa regenerated cellulose membrane and 350 μm channel spacer. The mobile phase was 0.025% FL-70 and 0.01% sodium azide made in deionized water at 18.2 MΩ-cm (Barnstead, USA). Separation of particles was performed using a cross flow of 0.75 mL/min and a channel flow of 1.0 mL/min. The AF4 eluent was plumbed directly through both the UV–vis and DLS detectors without any channel split. DLS measurements were performed in flow mode using a quartz flow-through cell (Hellma, Germany). Additional AF4 details are presented in Table 1.

Static DLS measurements of quantum dots, silver and gold nanoparticles were determined using a Brookhaven 90 Plus/BI-MAS instrument (Brookhaven Instruments, Holstville, NY, USA), as previously described [17]. Briefly, 2 mL samples were measured for nine minutes (three, 3 min replicates) using a scattering intensity weighted autocorrelation function, providing mean effective (hydrodynamic) diameters and one standard deviation. For the 10 nm nanogold, log normal distributions of intensity and particle weighted algorithms were compared to investigate the larger than expected hydrodynamic diameter obtained.

Table 1
Separation and detection instrument parameters used to measure nanoparticles by FFF techniques.

Symmetrical FFF–UV–ICP–MS/AES system	Postnova F-1000
Membrane	10 kDa regenerated cellulose
Channel and cross flow	1.0 and 0.75 mL/min, respectively
Injection volume	50 μL
Channel thickness	254 μm
Load time	15 s
Relaxation time	3.2 min
Approximate fractogram time (100 nm particle elution)	25 min
Asymmetrical FFF–UV–DLS system	Postnova AF-2000MT
Membrane	10 kDa regenerated cellulose
Channel and cross flow	1.0 and 0.75 mL/min, respectively
Injection volume	100 μL
Channel thickness	350 μm
Injection-focusing time	8 min
Approximate fractogram time (60 nm particle elution)	22 min
UV absorbance detector	Agilent 1100 VWD
Wavelength monitored	254, 395, 420, or 520 nm
Integration time	0.4 s
ICP–MS	Perkin Elmer Elan DRC II
Plasma power	1250 W
Nebulizer, spray chamber, and flow	MiraMist, Double Pass Scott, 0.85 L/min
Masses monitored (standard mode)	^{107}Ag, ^{109}Ag, ^{197}Au, ^{111}Cd, ^{66}Zn, ^{82}Se
Masses monitored (DRC mode)	^{111}Cd, ^{66}Zn, ^{78}Se, ^{48}SO, ^{107}Ag, ^{197}Au
DRC reaction gas and flowrate	Ultrapure oxygen, 0.7 mL/min
RPq for DRC mode	^{111}Cd=0.75, ^{66}Zn=0.75, ^{78}Se=0.75, ^{48}SO=0.55, ^{107}Ag=0.75, ^{197}Au=0.75
Dwell time per AMU	200–500 ms
Readings per replicate	1200–1800
ICP–AES	Perkin Elmer Optima 5300 DV
Plasma power	1400 W
Nebulizer, spray chamber, and flow	MiraMist, Cyclonic, 0.65 L/min
Plasma viewing mode	Axial
Wavelengths monitored	Ag 328.068 nm, Au 267.595 nm, Cd 228.802 nm, Zn 206.200 nm, Se 196.026 nm, S 180.669 nm
Integration time	5 s
Readings	300

2.3. Symmetrical FFF (SF4)

The SF4 instrument used for on-line interfacing with ICP–MS and ICP–AES was an F-1000 symmetrical FFF system from Postnova Analytics. It was interfaced to a Perkin Elmer Elan DRC II ICP–MS or a Perkin Elmer Optima 5300 DV ICP–AES by connection of the FFF effluent tubing directly to the MiraMist pneumatic nebulizer. An injection contact closure then triggered the ICP–MS to begin acquiring data. An Agilent 1100 variable wavelength detector was placed in-line between the SF4 and ICP systems to collect UV absorption data simultaneously. In addition to detection of the metal nanoparticles of interest, the UV detector data was also used for detection of NIST-traceable polystyrene bead size standards to convert retention time into particle size [42]. The SF4 system was equipped with a 10 kDa regenerated cellulose membrane and 254 μm channel spacer. The mobile phase consisted of a 0.025% sodium azide and 0.025% FL-70 surfactant dissolved in deionized water with a resistivity of 18.2 MΩ-cm; these instrumental conditions are similar to the asymmetrical system described above. Separation of the particles under investigation was achieved using a channel flow of 1.0 mL/min and a cross flow of 0.75 mL/min. The channel flow conditions allow direct connection of the SF4 effluent after the UV detector to the ICP–MS and ICP–AES nebulizers without the use of a flow splitter. Additional details of the SF4 separation conditions are also listed in Table 1.

The ICP–MS was operated in standard mode for the detection of silver, gold, and cadmium selenide quantum dots. However, to improve detection of selenium and allow the detection of sulfur in the quantum dots analyses, oxygen was used subsequently in the ICP–MS dynamic reaction cell to detect the more abundant ^{78}Se isotope and create the polyatomic species ^{48}SO. The dwell time per AMU was selected for each SF4 analysis such that one data point was collected per second. The number of readings per replicate was chosen such that data were collected for the entire length of the fractogram, usually for about 25 min. Table 1 also lists the operating conditions for the variable wavelength detector and ICP–MS.

The ICP–AES was operated with a nitrogen spectrometer purge to improve detection of low UV emission elements (e.g., Selenium and Sulfur), and generally used the most intense emission wavelength available. Integration time for each data point was 5 s to maximize detection of the transient signal. The number of readings was also chosen such that data were collected for the entire length of the fractogram, usually for about 25 min. Table 1 also lists the operating conditions for the ICP–AES.

3. Results and discussion

3.1. Gold and silver nanoparticles

To demonstrate size dependence response of the UV detector to various nanoparticles, UV absorbance spectra were collected of individual stock nanoparticles used. Shown in Fig. 1 are the UV–vis spectra obtained for the Au and Ag nanoparticles. The solution concentration was 16.7 mg/L for Au particles and 6.7 mg/L for Ag particles. The shift in wavelength maxima with increasing NP size is more pronounced for the Ag NPs as compared to the Au. This size dependent absorbance shift, assumed related to surface plasmon resonance changes as a function of size [47,48] makes it difficult to relate the UV peak area obtained in AF4–UV analysis to

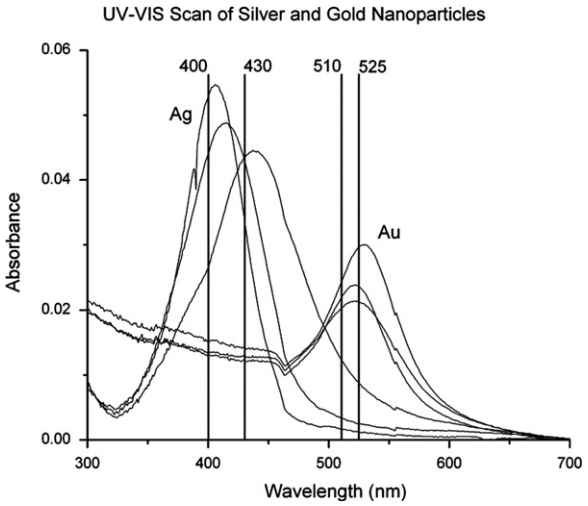

Fig. 1. Merged independent UV–vis scans of 10, 30 and 60 nm NIST gold nanoparticles stabilized in citrate (absorption maxima near 525 nm) and 10, 30, 60 nm Nanocomposix nanosilver particles stabilized in citrate (absorption maxima near 415 nm). Four wavelengths (400 and 430 for Ag, 510 and 525 for Au) are shown and correspond to UV wavelengths monitored in asymmetrical field flow fractionation with UV detection experiments.

the mass of particles eluting across the fractogram as shown in Fig. 2.

By choosing wavelengths where the UV absorbance is similar for each of the sizes (430 nm for Ag and 510 nm for Au) nearly similar peak areas are obtained (Fig. 2a and b). However, if one chooses a wavelength near the maximum for one particle size, in this case 400 and 525 nm for the 10 nm silver and gold, respectively, very different UV peak areas are obtained. Changes in UV response can be caused by changes in mobile phase and other analytical parameters, but also size [47–49]. One desirable feature of FFF is to quantify the amounts of NPs in mixtures, thus one can see that it would be very difficult if not impossible to relate AF4–UV response to mass for complex NP mixtures.

Online interfacing of dynamic light-scattering detectors can provide a means to obtain a measurement of NP size that is independent of the FFF retention time. In this case, the effect of size on detector response is even more pronounced (Fig. 3) due to the very strong dependence of scattering on particle size. As in the case of UV absorbance detection, online scattering detectors cannot be used to determine the mass concentration of the various components of a mixture. Furthermore, the use of dynamic light scattering to size NPs requires high concentrations, significantly above that used in this study to investigate the utility of on-line ICP–MS and ICP–AES. The hydrodynamic sizes

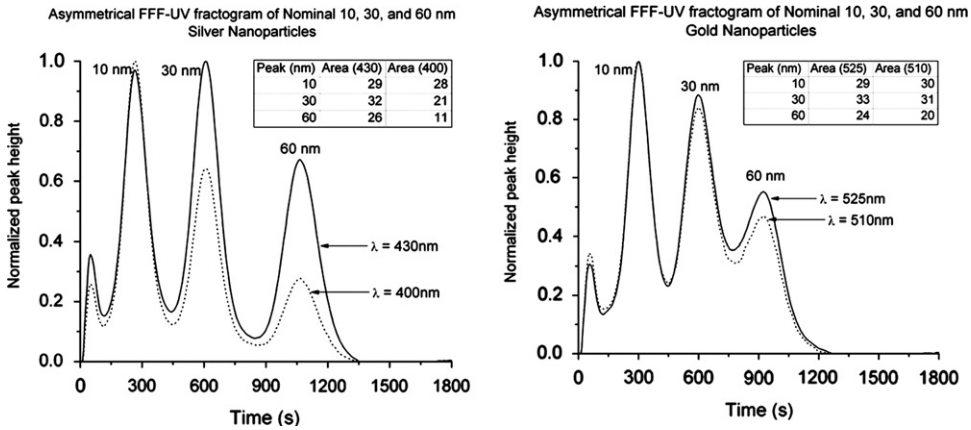

Fig. 2. Normalized absorbance for mixtures of 10, 30 and 60 nm nanogold and nanosilver particles separated by FFF with UV absorbance detection at two wavelengths for both particle types. Injection concentration was 16.7 mg/L for Au and 6.7 mg/L for Ag for each particle.

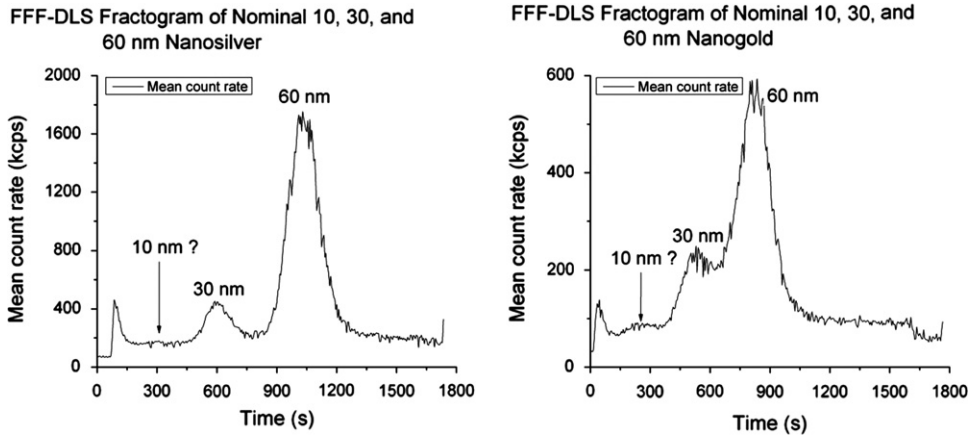

Fig. 3. DLS countrate (kcps) for mixtures of 10, 30 and 60 nm nanogold and nanosilver particles separated by FFF. These figures represent two analyses of three mixtures of the respective particle types. Injection concentration for Au was 16.7 mg/L and Ag was 6.7 mg/L for each particle. Due to insufficient sensitivity for the smallest particles, only 30 nm and 60 nm particles were observed.

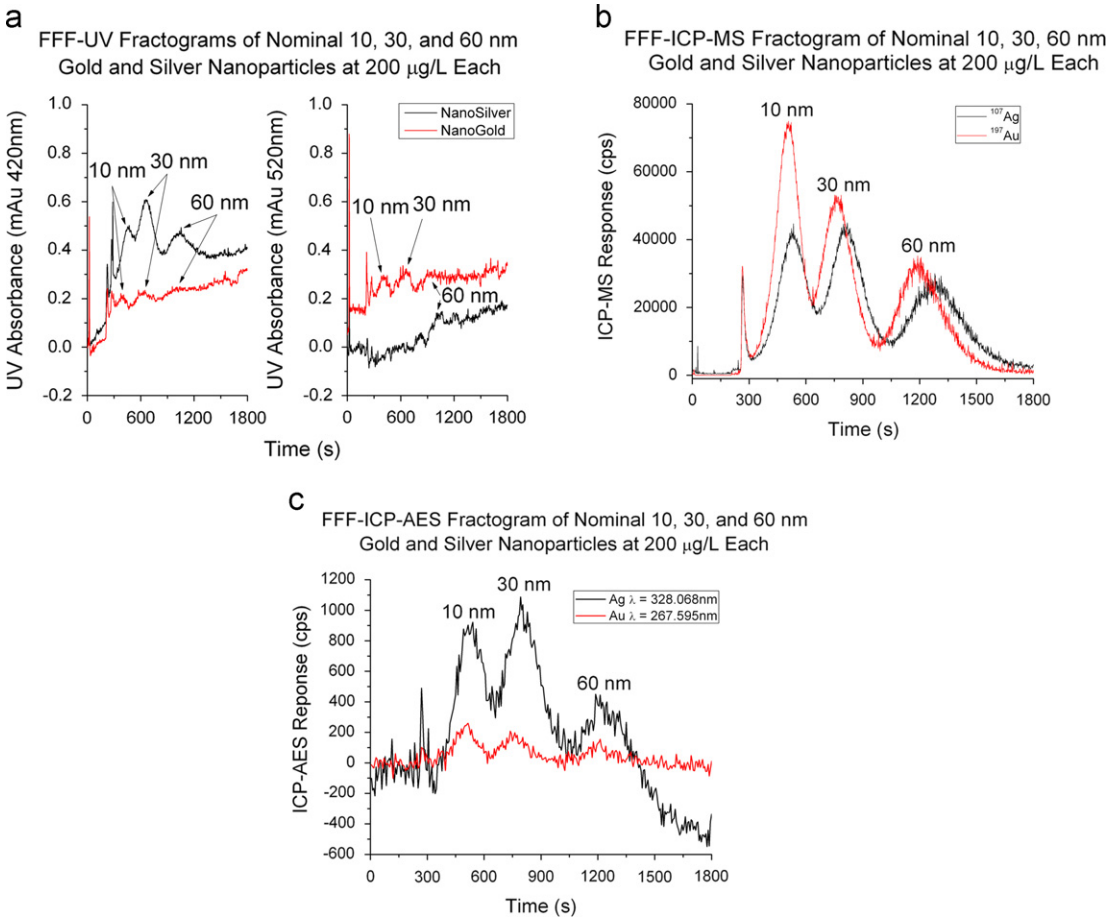

Fig. 4. FFF–UV, FFF–ICP–MS, and FFF–ICP–AES fractograms of six nanoparticle types at 200 μg/L concentration for each particle. The FFF–UV fractograms are composites plotted from four individual analyses of three particle mixtures (nanogold and nanosilver at two wavelengths), whereas the fractograms using the ICP–MS and ICP–AES are single analyses of a mixture of all six nanoparticles. The FFF–ICP–MS determined sizes for gold and silver were 18 and 18, 34 and 37, and 62 and 69 nm, respectively.

obtained by online DLS for the samples in Fig. 3 were unreliable and are not reported.

Use of ICP–MS and ICP–AES detectors' elemental specificity allows simultaneous detection of all six nanoparticle types mixed in a single solution. Fig. 4 shows SF4–UV, SF4–ICP–MS, and SF4–ICP–AES fractograms of nominally 10, 30, and 60 nm nanosilver and nanogold particles. Due to the non-selective nature of the UV detector, the data shown for the SF4–UV fractogram is a composite of four separate analyses: three mixed nanosilver particle types with UV detection at 420 nm, three mixed nanosilver particle types with UV detection at 520 nm, three mixed nanogold particle types with UV detection at 420 nm, and three mixed nanogold particle types with UV detection at 520 nm. In contrast to the UV absorbance data, however, use of ICP–MS and ICP–AES detectors' elemental specificity allows simultaneous detection of all six nanoparticle types mixed in a single solution. The SF4–ICP–MS and DLS determined particle sizes were similar, with the exception of the 10 nm gold which was more than 2-fold higher when measured by DLS. The SF4–ICP–MS determined sizes for gold and silver were 18 and 18, 34 and 37, and 62 and 69 nm, respectively. These values agree reasonably well with size determinations in single particle solutions by DLS for gold (31, 36, and 60 nm) and silver (22, 41, and 67 nm) [41,42]. The larger than expected DLS size for 10 nm gold was investigated by comparing a particle number versus the scattering intensity weighted autocorrelation, with the particle number function resulting in a much smaller hydrodynamic diameter (7 nm). This may suggest that impurities in the suspension or a few large particles skewed the DLS measurement to a larger size.

The superior detection capabilities of the ICP–MS are clearly evident in Fig. 4, compared to either ICP–AES or UV absorbance. The peak height for the ICP–MS fractogram suggests that a 1:20 dilution would still produce discernable peaks, resulting in estimated detection limits near 10 μg/L as previously reported [41,42]. However, despite the ICP–AES not being as sensitive as ICP–MS, the elemental specificity is superior to the UV absorbance results, and allows simultaneous detection of mixed gold and silver nanoparticles. Detection limits for gold nanoparticles by ICP–AES are near the 200 μg/L level shown in Fig. 4, however, the silver intensity is sufficient that a 1:2 dilution of this sample could still be measured, suggesting a detection limit around 100 μg/L. The use of NIST gold particles for size calibration (with or without ICP–MS or ICP–AES detection) in place of polystyrene beads and UV absorbance detection is possible based on these results, however, agreement between both types of size standards and detectors provides validity to the methodology.

3.2. *Quantum dots*

Multi-element detection capabilities may not always be needed for environmental studies where a pure phase is being added to model system. However, these sensitive techniques may be applicable to determining co-occurring constituents within a nanoparticle. Quantum dots represent a test case of a nanomaterial containing several metals that occupy different structural elements of the particle. The QDs tested below have a cadmium selenide core with a zinc sulfide shell, surrounded by a stabilizing

carboxylic functionalized organic coating. One property of QDs is absorption of UV radiation, and therefore the SF4–UV fractogram shown in Fig. 5 demonstrates a very strong response for these particles at 50 nM concentration. FFF sizing of these particles yields a hydrodynamic diameter of 27 nm, which agrees well with DLS measurements of ranging from 15 to 31 nm. The DLS analysis required a more concentrated solution (approximately 500 nM) than was required for FFF analysis (50 nM) and resulted in a second population of particle aggregates near 500 nm being the dominant population measured by DLS.

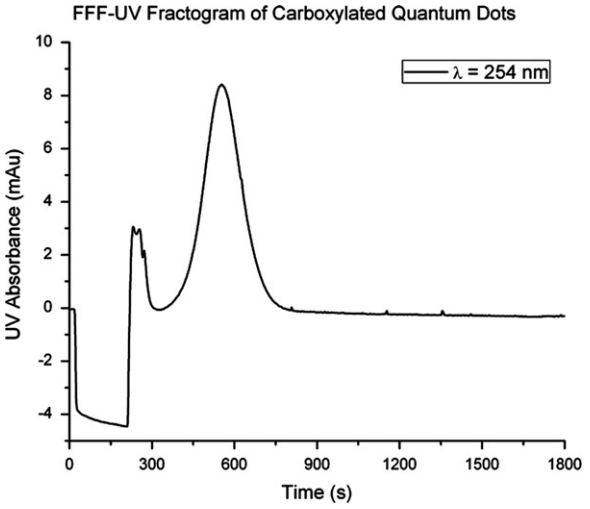

Fig. 5. FFF–UV fractogram of carboxylated CdSe–ZnS quantum dots with UV absorbance detection at 254 nm.

The fractogram in Fig. 5 shows excellent detection capabilities of the quantum dots by SF4–UV, but still suffers from lack of specificity, particularly if there are mixtures of particles present. Analysis of the same sample by SF4–ICP–MS and SF4–ICP–AES is shown in Fig. 6, and again demonstrates the advantages and limitations of these detectors. ICP–MS has superior detection capabilities compared to ICP–AES for cadmium and zinc, although both techniques are quite sensitive for these two elements. Standard mode ICP–MS, however, is unable to measure sulfur because of severe polyatomic interferences on all sulfur isotopes (particularly the most abundant, e.g., $^{32}O_2$ on ^{32}S), whereas ICP–AES can measure sulfur, although sulfur does not have a strong emission wavelength. Selenium is not particularly sensitive by either technique, due to the need to measure a low abundance isotope in ICP–MS (e.g., ^{82}Se) and the relatively weak selenium emission wavelength. Due to the sensitivity of Cd and Zn by both ICP–MS and ICP–AES, if only these two metals were used to detect the quantum dots shown in Fig. 7, it could be accomplished at levels 1000 and 100 times lower, respectively, than shown (approximately 0.05 and 0.5 nM, Cd and Zn concentrations of approximately 8 and 41 μg/L, respectively, which agrees relatively well with results for other metals described above and elsewhere [42]). Because the Se and S signals are substantially weaker than the Cd and Zn signals, detection of quantum dots at a level 10 times lower would represent Se and S concentrations of 0.172 and 4.39 mg/L, respectively, demonstrating for absolute

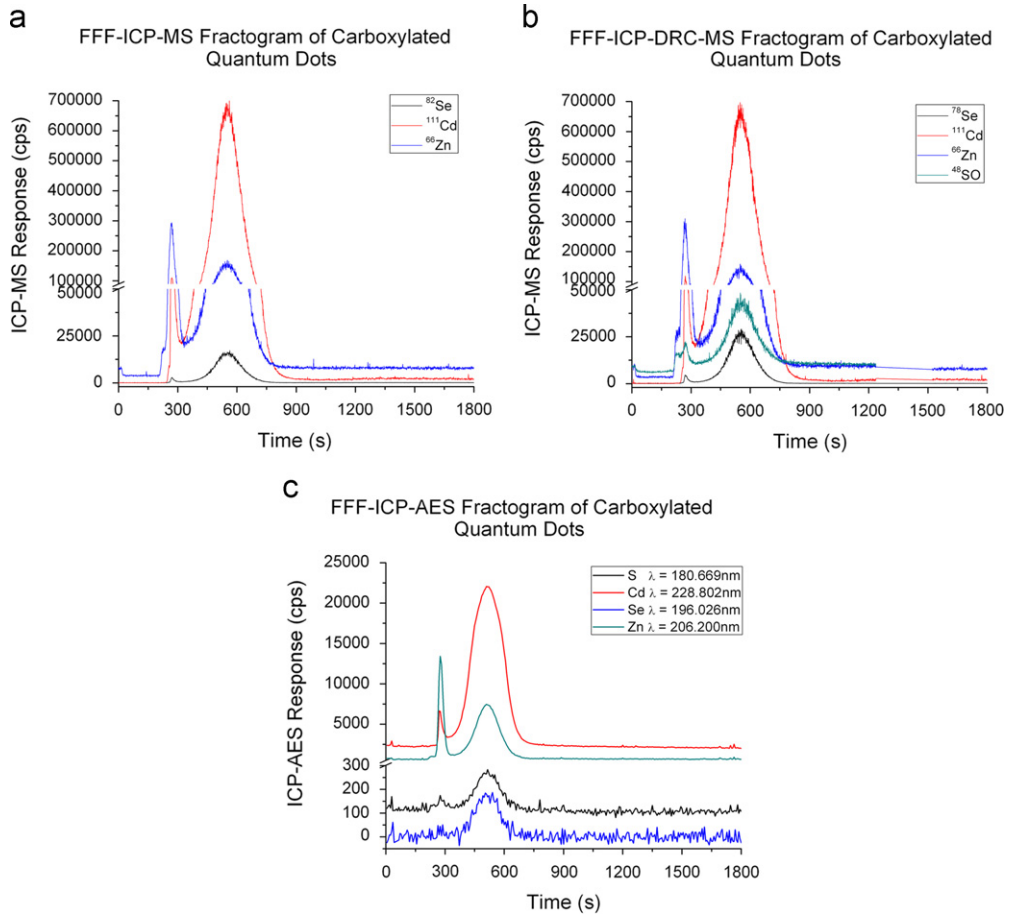

Fig. 6. FFF–ICP–MS, FFF–ICP–DRC–MS, and FFF–ICP–AES, fractograms of CdSe–ZnS core–shell quantum dots showing ability to measure 3- and 4-element components. The prominent void peak likely represents unreacted starting materials from the synthesis procedure.

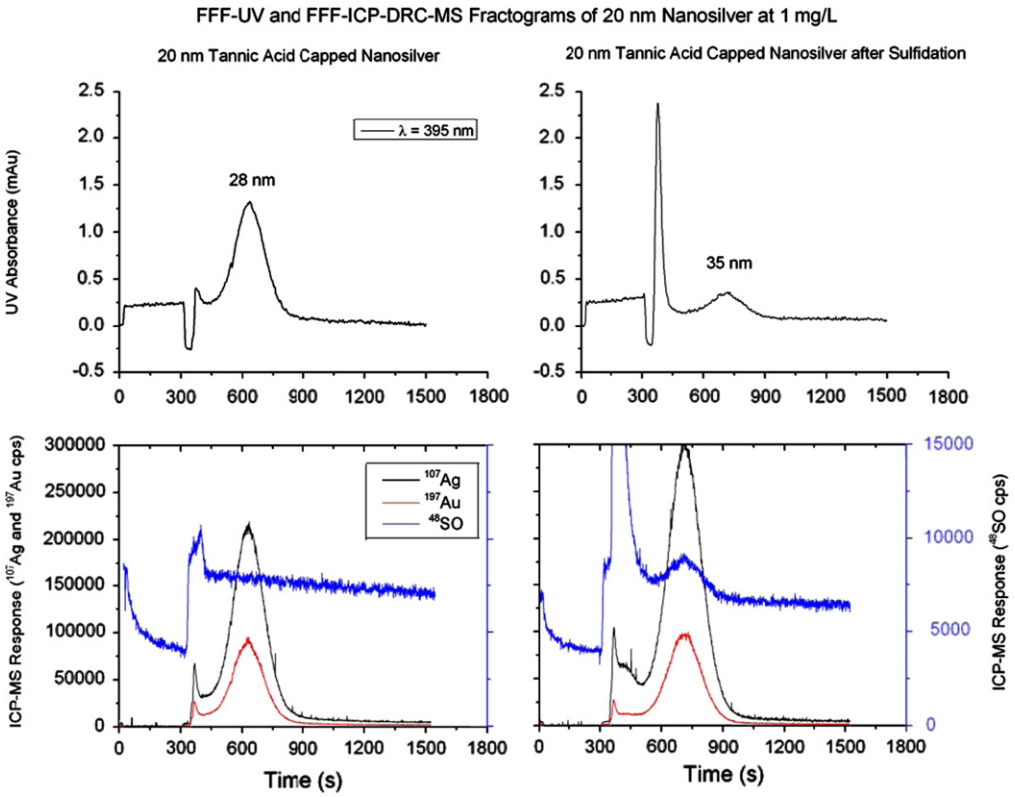

Fig. 7. FFF–UV and FFF–ICP–DRC–MS fractograms of tannic acid coated nanosilver with and without sulfidation.

detection, Cd and Zn represent the most sensitive candidates by either ICP–MS or ICP–AES.

Advances in ICP–MS technology, however, have included the addition of collision and reaction cells where gases are introduced post-plasma ionization to remove molecular interferences or create new molecular species to measure. This technology has been successfully applied for formation of oxide species in complex matrices [50]. For the current study, addition of oxygen to the dynamic reaction cell (DRC) is used to create a new polyatomic species ^{48}SO, to remove it from the $^{32}O_2$ major interferent. The SF4–ICP–DRC–MS fractogram of the quantum dot sample is also shown in Fig. 6.

Use of the oxygen reaction gas in the DRC also removes $^{78}Ar_2$ dimers formed in the plasma, thereby allowing detection of the more abundant ^{78}Se isotope, compared to ^{82}Se that is used in standard mode ICP–MS (23.78 vs. 8.73% abundance). Due to the high ionization potential of sulfur, and inefficiency in creating the oxygen polyatomic analyte, the signal intensity for ^{48}SO is only slightly better than the ICP–AES detection of the sulfur emission at 180.669 nm, but is a significant improvement over the standard ICP–MS method which could not detect all elements present in the nanoparticle. The DRC conditions listed in Table 1 were optimized for both selenium and sulfur, i.e., the oxygen flow rate of 0.7 mL/min was sufficient to remove all $^{78}Ar_2$ dimers with little loss of ^{78}Se signal, however, a higher oxygen flow rate will improve ^{48}SO formation, with a minimal loss of signal for the other three analytes (Fig. 5). These conditions were chosen to allow simultaneous detection of all species since it is not physically possible to switch between DRC and standard mode ICP–MS within a single transient FFF analysis. The ability to detect all four elements present in quantum dot nanoparticles by either ICP–AES or ICP–DRC–MS presents specific advantages to UV detection. The FFF provides sizing for the overall nanoparticle, however, if the ICP elemental signals are quantified, then relative sizes of the core–shell system can be estimated, providing additional structural information.

3.3. Silver nanoparticle sulfidation

The use of multi-element detection capabilities is further demonstrated by the application of SF4–ICP–DRC–MS analysis to silver nanoparticles that have undergone surface sulfidation. Due to the ability of silver (and other noble metals) to 'tarnish' when exposed to sulfide, being able to detect sulfur simultaneously with these nanoparticles provides a way to measure environmental aging [51–53]. Shown in Fig. 7 are a series of fractograms using UV and ICP–DRC–MS detectors of 20 nm tannic acid capped silver nanoparticles at 1 mg/L silver concentration with and without exposure to sodium sulfide (4:1 sulfur:silver molar ratio) for 4 days. The UV wavelength of 395 nm was chosen as this is the maximum absorbance wavelength for this specific nanoparticle. Because ICP–DRC–MS was shown in the previous quantum dot application to be slightly more sensitive than ICP–AES for sulfur detection, only it was used for the sulfur coating identification experiment.

The ICP–MS and reaction cell conditions for these analyses were optimized to maximize the detection of ^{48}SO specifically, and varied slightly from the conditions listed in Table 1, in order to maximize the detection of the minor sulfur component in this particle system. These modifications included the use of a cyclonic spray chamber, nebulizer flow of 0.95 L/min, and 1.0 mL/min oxygen flow rate in the DRC, all other conditions were the same as described above (Table 1). The elevated background signal for ^{48}SO, likely due to native Ca and S in the FL-70/sodium azide mobile phase and any $^{48}O_3$ formed in the reaction cell. Inefficiency in S ionization and oxide formation limit the ultimate ability to detect low μg/L concentrations of S in such analyses.

The particle size increases from approximately 27 to 35 nm during the sulfidation process, and is confirmed by both UV and ICP–MS detectors. However, there is a notable decrease in the UV signal, indicating that the surface plasmon resonance has changed with the development of the sulfide surface coating. Indeed, a UV–vis spectral scan of the sulfidized particles shows a maximum absorbance wavelength shift from 395 nm to approximately 225 nm. It is not entirely clear why the ICP–MS response increases after sulfidation, but may be due to the sulfide coating reducing the loss of particles to the FFF membrane. Indeed, the zeta potential measurement of the tannic acid coating silver nanoparticles became more negative (−7.6 mV for stock particles to −40.6 mV after sulfidation), indicating higher surface charge, and therefore stronger repulsion of the negative regenerated cellulose membrane. The particles do increase in mass (and size) (as determined by FFF retention time), possibly by precipitation of fresh silver sulfide on the surface of the particles from free silver in solution (generally reported to be in the 2–3% range [17]). This higher particle recovery is also supported by a slightly larger gold core signal observed in the post sulfidation fractogram, which is likely attributed to reduced loss of particles to the membrane, since there is no dissolved gold in the system to precipitate on the surface to make larger particles. The void peak observed in the sulfide-containing fractogram in Fig. 7 contains both sulfur and silver. The slight shoulder of the void peak could indicate the formation of small Ag_2S particles, yet no confirmatory information is available to discount unretained dissolved species.

The effect of sulfidation on these particles demonstrates the critical importance of tracking both particle size and composition, as both may change during exposure to environmental media [51,52]. Although the results in Fig. 7 are not yet quantitative, they do provide important qualitative information at near environmentally relevant concentrations. The SF4–ICP–DRC–MS fractograms shown in Fig. 7 also demonstrates the use of this technique to detect gold in silver nanoparticles. Silver nanoparticle synthesis can sometimes use nanogold 'seed' particles, which results in a gold core within the silver particle [54,55]. Due to the relative inertness of gold, this may not be a critical factor for toxicity or environmental studies, but does represent an ability to add quality control to manufacturing and purity analysis, as well as add a surrogate metal to aid in detection and tracking when using this technique. The gold concentration in the silver nanoparticles shown in Fig. 7 as determined by traditional ICP–MS analysis is approximately 20% of the particle, which is not necessarily an insignificant amount. Similar investigations of silver content in a variety of nanogold particles have been conducted, with results indicating small, yet detectable amounts generally less than 0.01% present. No matter how minute, the presence of silver in nanogold particles could confound toxicity studies (lethal median concentrations for nanosilver range from 2 to 126 μg/L, as total measurable silver [17]) where gold is intended as a nontoxic control nanoparticle.

4. Conclusions

Field flow fractionation is a powerful nanoparticle sizing technique. However, full exploitation of its capabilities requires the use of sensitive and selective analyte detectors. Interfacing the FFF separation method to ICP–MS, and to a lesser extent ICP–AES, provides the ability to detect and size nanoparticles at the μg/L level, a detection capability at least 10-fold lower than DLS or FFF–UV techniques. Shown in Table 2 are estimated detection limits of the various detectors evaluated in the current work as a function of nanoparticle constituents. These estimated detection limits are based on examination of the signal to noise ratio of the peak height to background and assume ideal conditions of pristine nanoparticles in simple media. Use of these hyphenated methods has been demonstrated in previous studies of complex environmental and biological systems. The additional information gained from the simultaneous elemental-specific nature of the detectors can identify co-occurring metals present in nanoparticles and can be used to track all constituents of a nanoparticle, including metal–nonmetal salts, as in the case of quantum dots or coatings resulting from environmental exposure. Additional work is underway to further improve capabilities, particularly of sulfur and possibly extend to chloride, to detect and ultimately quantify surface coatings of gold and silver nanoparticles at lower concentrations.

Table 2
Estimated detection limit (μg/L) for various metals in nanoparticle form by FFF separation using the various detectors described in the current work. Values determined by relative *S*/*N* ratio of FFF peak height to background and total measured metal by direct ICP–AES or ICP–MS analysis. This represents a conservative estimate because some constituents in each sample are present in the void peak rather than the particle peak.

FFF detector	Nanoparticle estimated detection limit (μg/L) by analyte					
	Au	Ag	Cd	Zn	Se	S
UV[a]	400	100	200	100	40	1,100
DLS[b]	4000	1500	NT	NT	NT	NT
ICP–MS	10	10	10	40	20	NA
ICP–DRC–MS	10	10	10	40	20	4,000
ICP–AES	200	100	80	200	200	10,000

NT— Not tested in this work.
NA—Sulfur cannot be analyzed by ICP–MS in standard mode due to interferences as described.
[a] Wavelength dependant, assumes particles remain intact.
[b] Nanoparticle size dependant, estimate given for 30 nm particles tested.

Acknowledgments

The use of trade, product, or firm names in this report is for descriptive purposes only and does not imply endorsement by the U.S. Government. The tests described and the resulting data presented herein, unless otherwise noted, were obtained from research conducted under the Environmental Quality Technology Program of the United States Army Corps of Engineers by the USAERDC. Permission was granted by the Chief of Engineers to publish this information. The findings of this report are not to be construed as an official Department of the Army position unless so designated by other authorized documents. The authors also thank Brandon Lafferty and David Johnson of the USACE for their editorial comments.

References

[1] N. Mueller, B. Nowack, Environ. Sci. Technol. 42 (2008) 4447–4453.
[2] F. Gottschalk, T. Sonderer, R. Scholz, B. Nowack, Environ. Sci. Technol. 43 (2009) 9216–9222.
[3] B. Nowack, Nano Today 4 (2009) 11–12.
[4] G.V. Lowry, K.B. Gregory, S.C. Apte, J.R. Lead, Environ. Sci. Technol. 46 (2012) 6893–6899.
[5] R.D. Handy, N. van den Brink, M. Chappell, M. Muehling, R. Behra, M. Dusinska, P. Simpson, J. Ahtiainen, J. Seiter, A. Bednar, A. Kennedy, T.F. Fernandes, M. Riediker, Ecotoxicology 21 (2012) 933–972.
[6] D.M. Mitrano, E.E. Lesher, A.J. Bednar, J. Monserud, C.P. Higgins, J.F. Ranville, Environ. Toxicol. Chem. 31 (2012) 115–121.
[7] H.E. Pace, N.J. Rogers, C. Jarolimeck, V.A. Coleman, C.P. Higgins, J.F. Ranville, Anal. Chem. 83 (2011) 9361–9369.
[8] A. Ulrich, S. Losert, N. Bendixen, A. Al-Kattan, H. Hagendorfer, B. Nowack, C. Adlhart, J. Ebert, M. Lattuada, K. Hungerbuhler, J. Anal. Atom. Spec. 27 (2012) 1120–1130.

[9] K. Tiede, A. Boxall, S. Tear, J. Lewis, H. David, M. Hassellov, Food Addit. Contam. 25 (2008) 795–821.
[10] G. Leppard, D. Mavrocordatos, D. Perret, Water Sci. Technol.: J. Int. Assoc. Water Pollut. Res. 50 (2004) 1.
[11] Y. Song, V. Jimenez, C. McKinney, R. Donkers, R.W. Murray, Anal. Chem. 75 (2003) 5088–5096.
[12] D.Y. Lyon, L.K. Adams, J.C. Falkner, P.J.J. Alvarez, Environ. Sci. Technol. 40 (2006) 4360–4366.
[13] K.W. Powers, M. Palazuelos, B.M. Moudgil, S.M. Roberts, Nanotoxicology 1 (2007) 42–51.
[14] K.A. Howell, E.P. Achterberg, A.D. Tappin, P.J. Worsfold, Environ. Chem. 3 (2006) 199–207.
[15] A. Akthakul, A.I. Hochbaum, F. Stellacci, A.M. Mayes, Adv. Mater. 17 (2005) 532–535.
[16] J.R. Lead, K.J. Wilkinson, Environ. Chem. 3 (2006) 159–171.
[17] A.J. Kennedy, M.S. Hull, A.J. Bednar, J.D. Goss, J.C. Gunter, J.L. Bouldin, P.J. Vikesland, J.A. Steevens, Environ. Sci. Technol. 44 (2010) 9571–9577.
[18] M. Hasselloev, J. Readman, J. Ranville, K. Tiede, Ecotoxicology 17 (2008) 344–361.
[19] J. Ranville, D. Chittleborough, F. Shanks, R. Morrison, T. Harris, F. Doss, R. Beckett, Anal. Chim. Acta 381 (1999) 315–329.
[20] J. Liu, J.D. Andya, S.J. Shire, AAPS J. 8 (2006) 580–589.
[21] F.A. Messaud, R.D. Sanderson, J. Runyon, T. Otte, H. Pasch, S. Williams, Prog. Polym. Sci. 34 (2009) 351–368.
[22] S.K. Ratanathanawongs, D. Lee, J. Sep. Sci. 29 (2006) 1720–1732.
[23] T. ChianÈa, N. Assidjo, P. Cardot, Talanta 51 (2000) 835–847.
[24] J.R. Lead, E.L. Smith, Environmental and Human Health Impacts of Nanotechnology, Wiley Online Library, 2009.
[25] M. Baalousha, J. Lead, Environ.Sci. Technol. 41 (2007) 1111–1117.
[26] R. Beckett, B.T. Hart, Environ. Part. 2 (1993) 165–205.
[27] M.H. Moon, D. Kang, J. Jung, J. Kim, J. Sep. Sci. 27 (2004) 710–717.
[28] J.C. Giddings, Science 260 (1993) 1456.
[29] C.W. Isaacson, D. Bouchard, J. Chromatogr. A 1217 (2010) 1506–1512.
[30] H. Hagendorfer, R. Kaegi, J. Traber, S.F.L. Mertens, R. Scherrers, C. Ludwig, A. Ulrich, Anal. Chim. Acta 706 (2012) 367–378.
[31] H. Hagendorfer, R. Kaegi, M. Parlinska, B. Sinnet, C. Ludwig, A. Ulrich, Anal. Chem. 84 (2012) 2678–2685.
[32] S. Dubascoux, I. Hecho, V. Hassellov, M.F. Kammer, M. Gautier, G. Lespes, J. Anal. Atom. Spectrom. 25 (2010) 613–623.
[33] L. Gimbert, K. Andrew, P. Haygarth, P. Worsfold, TrAC Trends Anal. Chem. 22 (2003) 615–633.
[34] M. Hassellov, F. von der Kammer, R. Beckett, Characterisation of aquatic colloids and macromolecules by field-flow fractionation, in: Wilkinson KJ, Lead JR (Eds.), Environ. Colloids Part.: Behav., Struct. Charact. (2007) 223–276.
[35] P. Reschiglian, A. Zattoni, B. Roda, E. Michelini, A. Roda, Fractionation Trend Biotechnol. 23 (2005) 475–483.
[36] B. Roda, A. Zattoni, P. Reschiglian, M.H. Moon, M. Mirasoli, E. Michelini, A. Roda, Anal. Chim. Acta 635 (2009) 132–143.
[37] S.K.R. Williams, J.R. Runyon, A.A. Ashames, Anal. Chem. 83 (2011) 634–642.
[38] M. Baalousha, B. Stolpe, J. Lead, J. Chromatogr. A 1218 (2011) 4078–4103.
[39] M. Bouby, H. Geckeis, F. Geyer, Anal. Bioanal. Chem. 392 (2008) 1447–1457.
[40] P. Krystek, A. Ulrich, C.C. Garcia, S. Manohar, R. Ritsema, J. Anal. Atom. Spec. 26 (2011) 1701–1721.
[41] H.E. Pace, E.K. Lesher, J.F. Ranville, Environ. Toxicol. Chem. 29 (2010) 1338–1344.
[42] A. Poda, A. Bednar, A. Kennedy, A. Harmon, M. Hull, D. Mitrano, J. Ranville, J. Steevens, J. Chromatogr. A 1218 (2011) 4219–4225.
[43] B. Schmidt, K. Loeschner, N. Hadrup, A. Mortensen, J.J. Sloth, C. Bender Koch, E.H. Larsen, Anal. Chem. 83 (2011) 2461–2468.
[44] S. Tadjiki, S. Assemi, C.E. Deering, J.M. Veranth, J.D. Miller, J. Nanopart. Res. 11 (2009) 981–988.
[45] M. Delay, T. Dolt, A. Woellhaf, R. Sembritzki, F.H. Frimmel, J. Chromatogr. A 1218 (2011) 42064212.
[46] M.F. Benedetti, J.F. Ranville, T. Allard, A.J. Bednar, N. Menguy, Colloids Surf. A 217 (2003) 1–9.
[47] J.R. Heath, Phys. Rev. B 40 (1989) 9982–9985.
[48] Y. Xiong, J. Chen, B. Wiley, Y. Xia, Y. Yin, Z.-Y. Li, Nanoletters 5 (2005) 1237–1242.
[49] T.J. Cho, V.A. Hackley, Anal. Bioanal. Chem. 398 (2010) 2003–2018.
[50] A.J. Bednar, Talanta 78 (2009) 453–457.
[51] C. Levard, B.C. Reinsch, F.M. Michel, C. Oumahi, G.V. Lowry, G.E. Brown, Environ. Sci. Technol. 45 (2011) 5260–5266.
[52] C. Levard, E.M. Hotze, G.V. Lowry, G.E. Brown, Environ. Sci. Techol. 46 (2012) 6900–6914.
[53] R. Kaegi, A. Voegelin, B. Sinnet, S. Zuleeg, H. Hagendorfer, M. Burkhardt, H. Siegrist, Environ. Sci. Techol. 45 (2011) 3902–3908.
[54] N.R. Jana, L. Gearheart, C.J. Murphy, Chem. Mater. 13 (2001) 2313–2322.
[55] L. Lu, H. Wang, Y. Zhou, S. Xi, H. Zhang, J. Hu, B. Zhao, Chem. Commun. 2 (2002) 144–145.